Hindawi
Shock and Vibration
Volume 2021, Article ID 2738627, 23 pages
https://doi.org/10.1155/2021/2738627

*Research Article*

# Numerical Analysis of the Effect of Heterogeneity on Underground Roadway Stability under Dynamic Loads

**Tao Guo, Hao Feng, Zequan Sun, Yang Zhao, Xingyu Wu, Xinggang Xu, and Lishuai Jiang**

*State Key Laboratory of Mining Disaster Prevention and Control, Shandong University of Science and Technology, Qingdao 266590, China*

Correspondence should be addressed to Lishuai Jiang; lsjiang@sdust.edu.cn

Received 23 July 2021; Accepted 11 September 2021; Published 23 September 2021

Academic Editor: Arturo Garcia-Perez



With the increasing depth of coal mining and expanding mining scale, the rocks surrounding deep roadways are in a complex mechanical condition of frequent dynamic disturbance. The heterogeneity has an important influence on rock mass failure under dynamic loads. Therefore, it is necessary to study the deformation and failure of heterogeneous roadway under dynamic load. In this paper, the effect of heterogeneity on stability of roadway under static and different dynamic loads is studied. According to the results, the effect of rock mass heterogeneity on the deformation and failure of surrounding rock varies with different degrees of heterogeneity. Under static loading conditions, the stability of roadway is negatively correlated with the degree of heterogeneity of the rock mass. Under dynamic loading conditions, the change of heterogeneity degree has significant influence on the stability of surrounding rock. With the increase in dynamic load strength, the change in variation difference in the average value of roof sag, stress distribution, and plastic zone caused by variations in heterogeneity will increase. This study contributes to understanding the deformation and failure characteristics of heterogeneous roadways under dynamic loads and can be used to analyze heterogeneous roadways under dynamic loads.

## 1. Introduction

In underground coal mining, due to increasing depletion of shallow resources, mines have entered the state of deep resource mining domestically and internationally. Meanwhile, deep roadway surrounding rock is under a complex stress condition. With dynamic disaster accidents becoming increasingly serious, the deep roadways show a trend of large damage. Maintenance of deep roadway has become more difficult, which seriously hindered the safe production and economic benefits of the coal mine [1]. According to statistical data, more than 80% of roadways in mines are dynamic pressure, affected by the microseismic events and mining tremors; the dynamic pressure roadway is frequently disturbed by dynamic load [2].

Based on the above situation, research studies on the mechanism and control of underground roadway instability under dynamic loads have received extensive attention from domestic and foreign scholars [3–9]. He et al. [10] discussed the distribution characteristics of static and dynamic loads near the working face and proposed the stress condition and energy variation law. Kong et al. [11] conducted the possibility analysis of the occurrence of roadway rock burst under different dynamics. Liu et al. [12] analyzed the judgment formula for failure of compound coal-rock under static-dynamic coupling stress and proposed a formula for energy release of compound coal-rock, revealing that the interaction between the structure of compound coal-rock and static-dynamic coupling stress is the key to rock burst. Numerous efforts have been made to investigate the control of underground roadway instability under dynamic loads. However, most researchers assumed that the rock mass is homogeneous in their studies. Based on complex deep mining conditions, the lithology of coal seam strata is relatively weakly affected by sedimentation, and the rock mass is weakened as a result of fracture development, which leads

to high heterogeneity in the rocks surrounding deep roadways. As shown in Figure 1, the roadway has remarkable heterogeneity characteristics and the assumption of a homogeneous rock mass is improper.

Regarding research on heterogeneous methods, in recent years, numerical simulation, as an advanced technique, has provided a new way to study rock heterogeneity [13–18]. On the one hand, numerical simulation has the advantage of controllability. Through software built-in commands, the degree of heterogeneity of the rock mass can be changed. On the other hand, numerical simulation, compared with laboratory test [19–21], breaks through the limit of the specimen size [22–24]. The numerical simulation can simulate large engineering scale heterogeneous rock mass. Therefore, to clearly investigate the characteristics of heterogeneous roadways under dynamic loads, this study can use the numerical simulation research method, which considers rock mass heterogeneity and complex stress conditions. Based on Zhaogu No. 2. mine, the effect of heterogeneity on rock mass stability under dynamic loads is analyzed. The research results can provide a method technology and provide some help for selecting suitable support scheme for further study of other highly heterogeneous rock engineering projects that are frequently disturbed by dynamic loads.

## 2. Engineering Case

*2.1. Geotechnical Conditions of the Zhaogu No. 2 Mine.* The average thickness of coal seam is 6.0 m and buried depth is about 625 m. The transportation roadway of 11030 working face in Zhaogu No. 2 mine is the research object and is shown in Figure 2 [25].

The roadway excavation along the roof and the designed rectangular section has a width × height of 5.2 m × 4.0 m. The supporting design parameters and size of the roadway are shown in Figure 3. The roof and ribs' bolts are supported by high-strength rebar bolts; the spacing between rows is 800 mm × 800 mm. The roof cable bolts use steel strands, with a row spacing of 1300 mm × 800 mm.

*2.2. Deformation Characteristics of Heterogeneous Roadway.* In complex stress environments, the degree of rock mass heterogeneity directly affects the stability of underground roadways. In engineering practice, a heterogeneous rock mass will be affected by various forces during excavation, and underground roadways will be further damaged. As shown in Figure 4, the surrounding rock of the 11030 panel entry is a typical heterogeneous rock mass. The surrounding rock marked by red has large deformation, but the surrounding rock marked by green is relatively intact. Through field monitoring, it is discovered that the surrounding rock is seriously broken, which is only affected by excavation. The sag of the roof is large, and the two ribs have significant inward convergence.

Due to existence of discontinuities in surrounding rock, the distribution of fractures leads to heterogeneity of rock mass in space. The deformation of the surrounding rock shows significant heterogeneity. This heterogeneous large deformation reduces the supporting effect.

*2.3. Field Deformation Monitoring.* Data are obtained through field monitoring, which can be used to quantitatively study the stability of the roadway. Therefore, the displacement of the target roadway was monitored for more than 70 days. The measurement method is carried out by measuring the variation of surrounding rock. The layout of displacement measuring points is shown in Figure 5. The station layout is shown in Figure 6. The displacement data were measured with a tape measure and the absolute and relative shifts were calculated, respectively. Measurement position scheme is shown in Table 1. Seven of the convergences (D1 to D7) were monitored, as shown in Figure 7.

Statistical analysis of data from the monitoring stations is shown in Table 2. The displacement data show that the surrounding rock experienced serious deformation during the monitoring period. Roof sag was 150 to 208.8 mm, and horizontal convergence reached 355 to 402 mm. There are obvious differences in the deformation at different measuring stations. The maximum difference in roof sag is 64.7 mm, and the maximum difference in rib displacement is 32.4 mm. By comparing the data in different time periods, it is found that, in the first 20 days, the deformation of the roof and two ribs is relatively intense and the deformation rate is large, the deformation rates at different measuring stations are significantly different, and the deformation of the surrounding rock shows significant heterogeneous distribution characteristics.

## 3. The Establishment of Heterogeneous Model

*3.1. The Weibull Distribution.* Heterogeneity, as an important characteristic of rock masses, affects the structural stability and failure pattern of rock masses and needs to be fully considered in numerical simulations. According to previous studies [26–29], the Weibull distribution function can effectively characterize surrounding rock with heterogeneous characteristics.

The Weibull distribution formula is as follows:

$$f(u) = \frac{m}{u0}\left(\frac{u}{u0}\right)^{m-1} \exp\left[-\left(\frac{u}{u0}\right)^{m}\right], \quad (1)$$

where $u$ is the mechanical property, $u_0$ is the average value of the mechanical property, and $m$ is the homogeneity index. The higher $m$ is, the higher the degree of rock mass homogeneity is. Rock mass tends to be homogeneous when $m$ reaches infinity [24]. In this study, using the strain-softening model of FLAC3D with the second development of FISH, we assign properties of rock elements based on the Weibull distribution. The simulated flow diagram is shown in Figure 8.

*3.2. Model Description.* In this numerical model, an important factor that agrees with field practice has been considered, which is the heterogeneity of rock. According to

Figure 1: The roadway with heterogeneity characteristics.

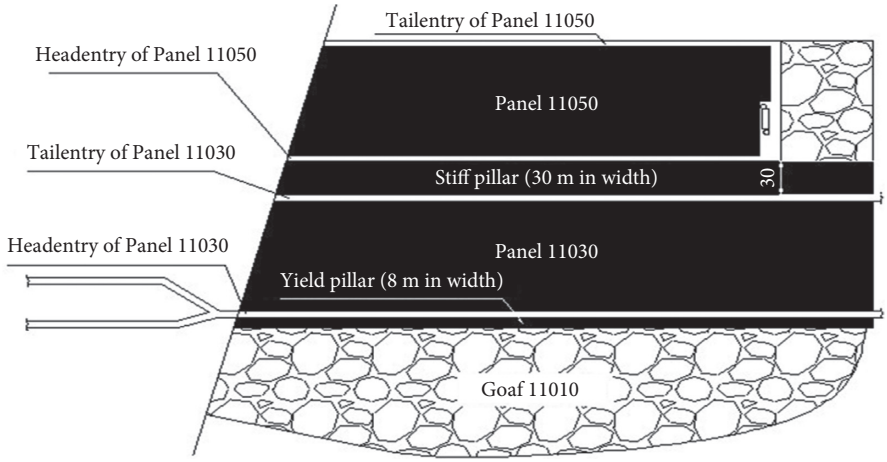


Figure 2: Panel layout.

the sensitivity analysis of the model grid density, the size of the model is determined to be $60 \times 60 \times 60$ m, as shown in Figure 9. In situ stresses are applied; according to a previous numerical study of the same roadway [30], we apply 15 MPa vertical stress to the top of the model to simulate the overburden pressure, and the horizontal-vertical stress ratios were set at 0.8 and 1.2, respectively. No displacement is allowed in the direction perpendicular to the side boundaries. The mechanical parameters of rock mass are listed in Table 3 [31].

In order to verify the rationality of deformation distribution studied in this paper, comparative analysis of simulation results and field data found that the simulation results ($m = 1.96$) mostly match the field monitoring results, as shown in Figure 10. Therefore, this model can be used for subsequent research.

*3.3. Method of Applying Dynamic Load.* In the dynamic calculation of numerical simulation, it is important to choose a reasonable dynamic load application method and conditions. At present, it is believed that the occurrence of dynamic disaster accidents is closely related to the propagation of vibration waves in rock masses. However, it is very difficult to determine the position of the dynamic load source. Actually, the stress wave acting on the surrounding rock is a complex stress wave that has undergone multiple interference or reflection. Thus, it is difficult to study with the method of theoretical analysis. According to elastic wave theory, any complex stress wave can be obtained by the Fourier transform of one or more sine functions [32, 33]. Therefore, we can use sine waves to simulate the dynamic load.

The sine shock wave formula is as follows:

$$v(z,t) = v_0 \sin\left[2\pi f\left(\frac{t-z}{c}\right)\right], \tag{2}$$

where $v_0$ is the maximum vibration velocity of the particle and $f$ is the shock wave frequency. Note that dynamic load damping induced by inner friction of materials cannot be ignored. Research shows that the dynamic analysis of rock mechanics by using local damping can achieve ideal results. The local damping of rock is generally selected in the 2% to 5% range. The damping ratio for this experiment is chosen to be 5%. Waves transiting the surrounding rocks will generate a particle vibration velocity, and the maximum vibration

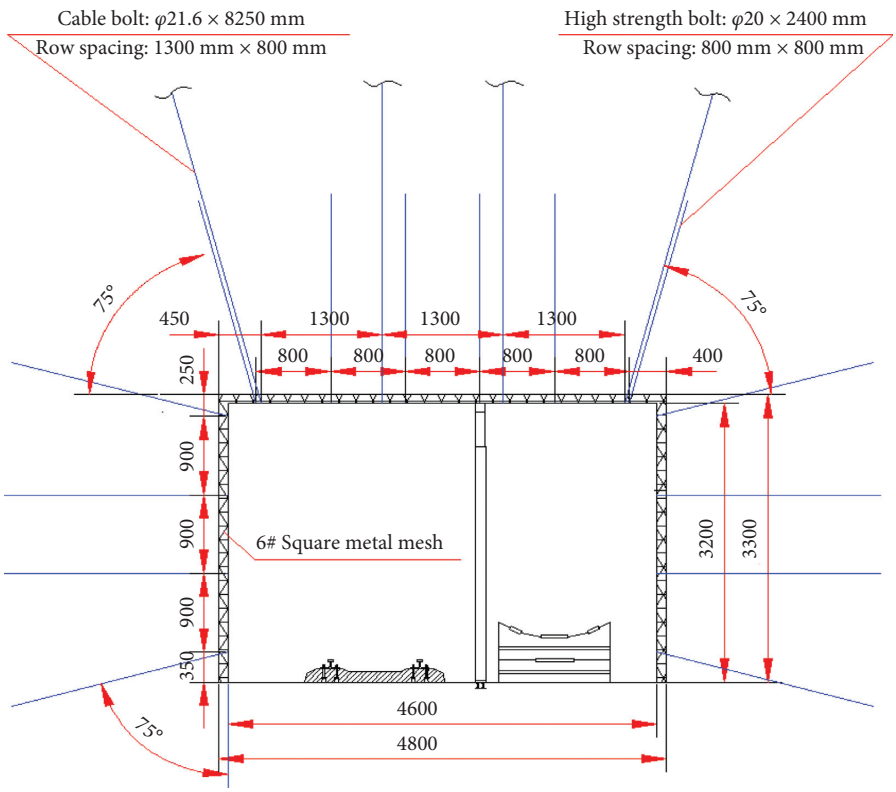


Figure 3: Support design.

(a)

(b)

Figure 4: Large deformation of a heterogeneous roadway during excavation.

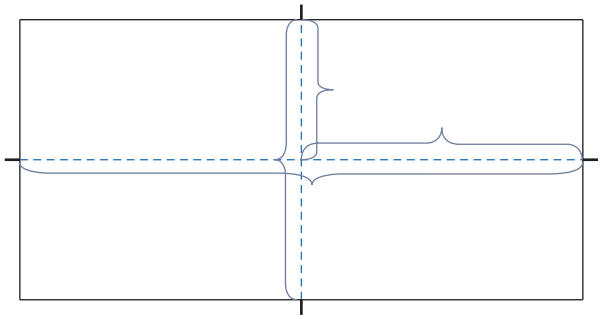

Figure 5: Layout of displacement measuring points.

velocity is called the peak particle velocity (PPV). Some researchers have conducted statistical analysis of the dynamic disasters in different coal levels, and the data show that the average PPV is 2.5 m/s [34]. Therefore, the applied dynamic load is determined according to previous research, since this is a general research and not a case study. So, we did not determine the dynamic load according to one specific seismicity event, but a reasonable load to present a general condition.

## 4. Effect of Rock Mass Heterogeneity on Underground Roadway Stability under Static Loads

The rock mass has strong heterogeneity due to heterogeneously distributed fractures. Not only does the heterogeneity of the rock mass impacts significantly the stability of the rock mass structure but also makes underground engineering more complicated.

To comprehensively investigate the stability of heterogeneous roadways, the roof deformation distribution, deformation magnitude, stress distribution, and surrounding rock plastic zone were monitored.

*4.1. Effect of Rock Mass Heterogeneity on Roof Deformation under Static Loads.* Under static loading conditions, spatial distribution pattern of roof sag for different $m$ is shown in Figure 11, and the positions of the maximum sag are marked in red.

The effect of rock mass heterogeneity on roof deformation is reflected in two sides: deformation magnitude and spatial distribution pattern. In a low heterogeneity scenario, the roof deformation distribution in space shows strong heterogeneity, and the positions of the maximum sag have significant randomness. When $m = 1$, the maximum roof sag is the largest, followed by $m = 3$, and when $m = 100$, the maximum roof sag is the smallest. As $m$ increases, the maximum roof sag decreases from 119.5 mm to 48 mm.

The variation with $m$ in the roof sag and deformation distribution characteristics is caused by the heterogeneous distribution in mechanical properties of the rock mass. As the rock mass becomes more heterogeneous, the deformation tends to be nonuniformly distributed because heterogeneously distributed fractures lead to heterogeneous rock mass weakening, resulting in severe deformation and instability.

To study the effect on the roof sag of the rock mass heterogeneity induced by heterogeneously distributed fractures, studies on roof deformation are performed in different $m$. Figure 12 shows the changes in the deformation distribution pattern and the variation of average roof sag with $m$. Figures 11 and 12 show that there are distinct differences in the deformation distribution pattern with different $m$.

As seen in the deformation distribution pattern results of Figure 12, when $m = 1$, the deformation distribution of the roof is mainly concentrated in the range of 80~99.9 mm and 100~119.9 mm (53.1% and 34.3%, respectively). When $m = 3$, $m = 5$, and $m = 100$, the deformation distribution of the roof is mainly concentrated in the range of 30~59.9 mm (89%, 96.8%, and 100%, respectively). The heterogeneity of the rock mass affects the deformation distribution pattern. The effect on the deformation distribution pattern caused by variations in heterogeneity will be weakened with an increase in $m$. As demonstrated with the data analyses and shown in Figure 12, with increasing $m$, the strength of the surrounding rocks is improved and the average roof sag decreases from 95.1 to 37.6 mm. Moreover, the stability of the roof is improved, and the deformation tends to be uniformly distributed.

*4.2. Effect of Rock Mass Heterogeneity on Stress Distribution of Roof under Static Loads.* In order to investigate the effect of rock mass heterogeneity on the stress state of the roof, the vertical stress distribution and local stress characteristics of the roof are analyzed.

Under static loading conditions, the vertical stress distribution of the roof is shown in Figure 13. The rock heterogeneity has a large effect on the vertical stress distribution. As the rock mass becomes more homogeneous, the vertical stress distribution tends to be uniformly distributed. These results indicate that the heterogeneity of the rock mass leads to strength variations in different positions of the roof, and the areas with low strength must evolve into weak spots in the roof. Under static loading conditions, these areas with low strength will be primarily damaged for stress release, and the stress value decreases in the local range. Therefore, the roof is affected by the rock mass heterogeneity, forming regions where the stress decreases locally. As demonstrated with the data analyses and shown in Figure 13, when $m = 1$, the stress reduction region in the roof is 9.4% of the total area and the value of the stress reduction is 0.5 MPa; when $m = 5$, the stress reduction region is 2.8% of the total area and the value of the stress reduction is 0.6 MPa; when $m = 100$, the vertical stress in the roof is uniformly distributed with a value of 0.6 MPa. The higher the degree of rock mass heterogeneity is, the larger the effect of the vertical stress distribution will be. As the degree of rock mass heterogeneity decreases, the size of the local stress reduction region will become larger, and the magnitude of the stress reduction will be smaller.

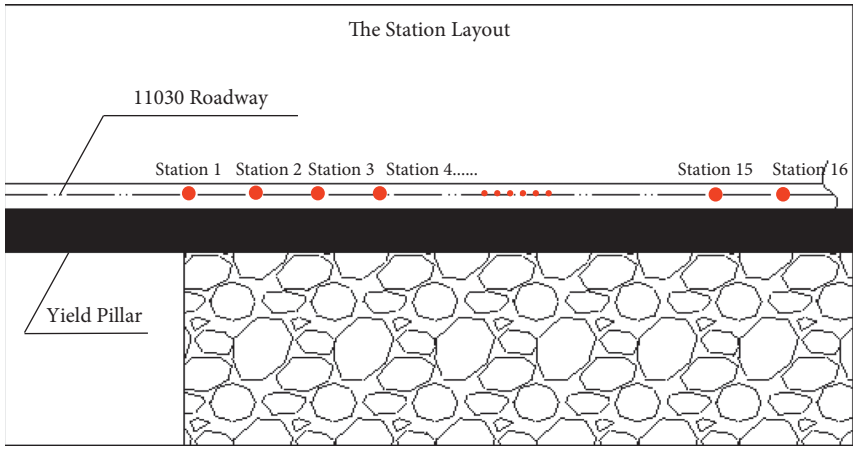


Figure 6: Layout of stations.

Table 1: Positions of measuring points for displacement.

| Number | Location (m) |
|---|---|
| 1 | 105 m to roadway opening |
| 2 | 115 m to roadway opening |
| 3 | 125 m to roadway opening |
| 4 | 135 m to roadway opening |
| 5 | 145 m to roadway opening |
| 6 | 155 m to roadway opening |
| 7 | 165 m to roadway opening |
| 8 | 175 m to roadway opening |
| 9 | 185 m to roadway opening |
| 10 | 195 m to roadway opening |
| 11 | 205 m to roadway opening |
| 12 | 215 m to roadway opening |
| 13 | 225 m to roadway opening |
| 14 | 235 m to roadway opening |
| 15 | 245 m to roadway opening |
| 16 | 255 m to roadway opening |

According to the data analysis in Figures 11 and 13, the initial stress state of the rock mass has been disturbed due to roadway excavation, resulting in the release and redistribution of the stress. The higher the degree of heterogeneity is, the more heterogeneous the distribution of mechanical properties and the weaker the mechanical properties of the rock mass will be. Failure will occur at relatively lower strength areas, and the stress in these areas transfers to the adjacent regions. Meanwhile, this effect leads to severe roof deformation and failure in the adjacent regions until the stress in the surrounding rocks reaches the equilibrium state. When the degree of rock mass homogeneity is higher, the mechanical properties tend to be uniformly distributed. Therefore, the strength of the roof is in a relatively close range, and there will be no weak areas caused by the excessive strength difference in the roof.

*4.3. Effect of Rock Mass Heterogeneity on Plastic Zones under Static Loads.* In the study of roadway stability, the extent of plastic zone is an important parameter to analyze the stability of surrounding rock. The distribution of the plastic zone directly determines the failure pattern and failure degree of the roadway. To comprehensively study the characteristics of the plastic zone in a heterogeneous roadway, monitoring sections are arranged at different positions of the roadway, and three representative sections are selected for analysis, as shown in Figure 14. Along the roadway excavation direction, the roadway monitoring sections at 22 m, 26 m, and 36 m are marked in red, green, and blue, respectively.

In order to investigate the effect of rock mass heterogeneity on the plastic zone of surrounding rocks, the plastic zone of the roadway at different positions under static loads is analyzed, as shown in Figure 15.

The rock mass heterogeneity has a large effect on the plastic zone of the roadway. At the same position of the roadway, the range of the plastic zone decreases significantly with the increase of $m$. Taking the plastic zone at 22 m as an example, investigations on the effect of heterogeneity in the plastic zone of the roadway are performed. When $m = 1$, the mechanical properties of the rock mass tend to be heterogeneously distributed, the strength of the surrounding rocks is low, and the extent of the plastic zone is large. The plastic zone extent of roof and floor are 5.0 m and 7.8 m, respectively, and discrete fracture elements are found. When $m = 5$, the strength of surrounding rocks is improved, resulting in the decrease of plastic zone extent, as the plastic zone extent of the roof and the floor are 4.0 m and 6.9 m, respectively. When $m = 100$, the mechanical properties of rock mass tend to be distributed homogeneously, the strength of surrounding rocks becomes higher, and the plastic zone extent continues to decrease. The plastic zone extents of the roof and floor are 2.0 m and 4.4 m, respectively. The discrete fracture elements in the plastic zone have disappeared.

At the different positions of the roadway, the extent of the plastic zone with the same values of the homogeneity index $m$ is different. By studying the characteristics of the plastic zone at different positions, the extent of the plastic zone on the right rib of the roadway and the number of failure elements are analyzed. When $m = 1$, the extent of plastic zone on the right rib of roadway (20 m, 26 m, and 36 m) is 6.6 m, 7.2 m, and 6.0 m, respectively, and the maximum change is 1.2 m. When $m = 5$, the extent of the plastic zone on the right rib of roadway (20 m,

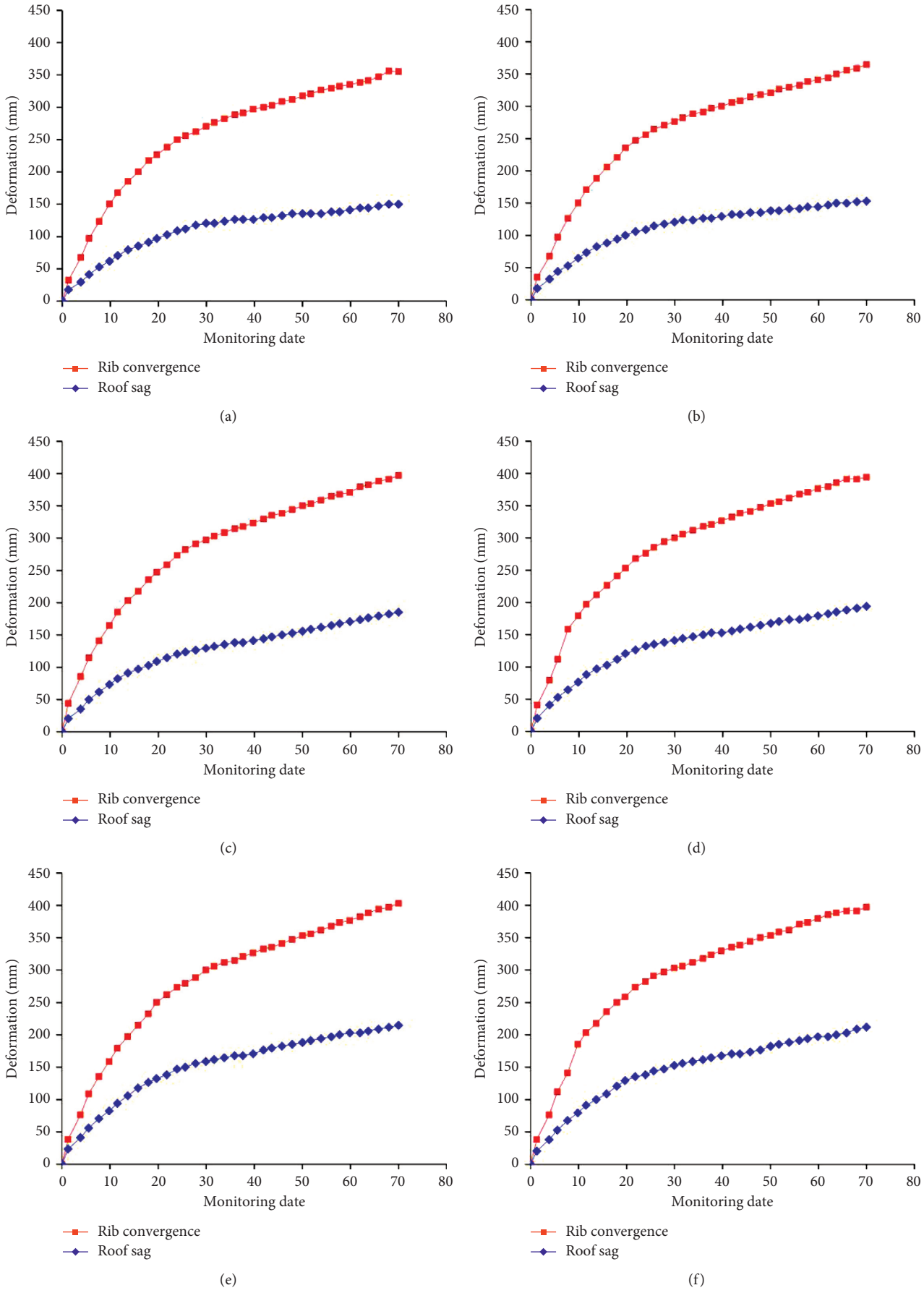


Figure 7: Continued.

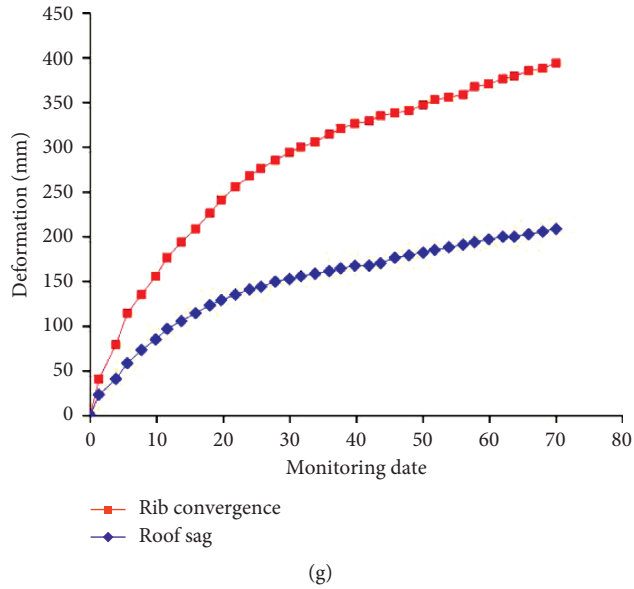


(g)

Figure 7: Monitoring the surface displacement curves. (a) D1; (b) D2; (c) D3; (d) D4; (e) D5; (f) D6; (g) D7.

Table 2: Surface displacement data of surrounding rock.

| Stations | Roof | | | | Two ribs | | | |
|---|---|---|---|---|---|---|---|---|
| | Value of sag (mm) | The cumulative sag of the first 20 d (mm) | The cumulative sag of 20~50 d (mm) | The cumulative sag of 50~70 d (mm) | Value of convergence (mm) | The cumulative convergence of the first 20 d (mm) | The cumulative convergence of 20~50 d (mm) | The cumulative convergence of 50~70 d (mm) |
| *D*1 | 150 | 97.0 | 38.2 | 14.8 | 355 | 226.4 | 91.2 | 37.4 |
| *D*2 | 152.9 | 100 | 3 8.2 | 14.7 | 364.7 | 235.2 | 85.2 | 44.3 |
| *D*3 | 185.2 | 108.8 | 47.1 | 29.3 | 397 | 247.0 | 102.9 | 47.1 |
| *D*4 | 194.1 | 120.6 | 47.1 | 26.5 | 394.1 | 252.9 | 100.0 | 41.2 |
| *D*5 | 214.7 | 132.4 | 55.8 | 26.5 | 402.9 | 250.0 | 102.9 | 50.0 |
| *D*6 | 211.7 | 129.4 | 52.9 | 29.4 | 397.0 | 258.8 | 94.1 | 44.1 |
| *D*7 | 208.8 | 129.4 | 52.9 | 26.5 | 394.1 | 241.2 | 105.8 | 47.1 |

26 m, and 36 m) is 6.6 m, 6.6 m, and 6.0 m, respectively, and the maximum change is 0.6 m. When $m = 100$, the extent of the plastic zone on the right rib of roadway (20 m, 26 m, and 36 m) is 6.0 m, 6.0 m, and 6.0 m, respectively. With an increase in $m$, the variation in plastic zone extent at different positions of the roadway gradually decreases.

Moreover, the number of failure elements in surrounding rock is analyzed by development program. The number of failure elements at different positions for different values of $m$ is listed in Table 4. When $m = 1$, a large number of failure elements have been found in the roof and floor of the roadway, and the plastic zone is asymmetrically distributed. Due to the heterogeneous distribution of mechanical properties in rock mass, the number of failure elements in the plastic zone at different positions varies significantly, and the maximum difference in the number of failure elements at different positions is 223. When $m = 5$, the mechanical properties of rock mass are improved, and the total number of failure elements in the plastic zone at different positions is reduced, but the plastic zone at different positions still presents asymmetric characteristics. When $m = 100$, the rock mass tends to be homogeneous due to homogeneously distributed fractures, and the number of failure elements in the plastic zone at different positions decreases. The maximum difference in the number of failure elements at different positions is 12, and the characteristics of asymmetrical failure in the plastic zone at different positions disappear. The influence of the change in position on the number of failure elements in each plastic zone will gradually weaken with an increase in $m$.

Notably, the above plastic zone changes are due to the heterogeneity of the rock mass. Because the size of roadway is often much longer than the width, roadway is usually assumed to be plane strain condition in the analysis of roadway stability. However, the assumption is made that the rock mass is homogeneous, ignoring the effect of rock mass heterogeneity on the plastic zone at different positions. The plastic zones at different positions of the roadway are significantly different when the rock mass heterogeneity is considered. Therefore, it is necessary to consider the effect of rock mass heterogeneity on the plastic zone in numerical simulations.

According to the comparative analysis, it is important to consider the heterogeneity of rock masses when studying

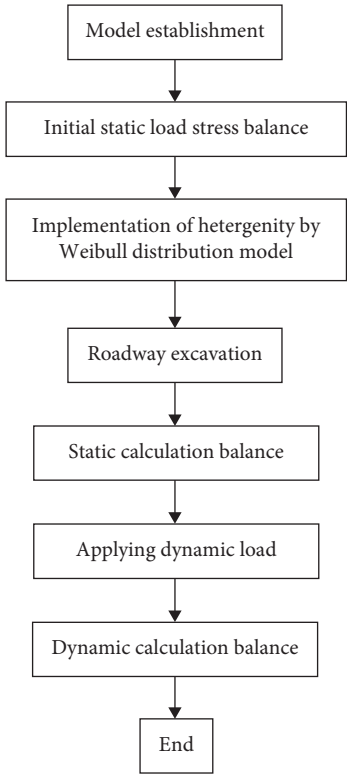


Figure 8: The simulated flow diagram.

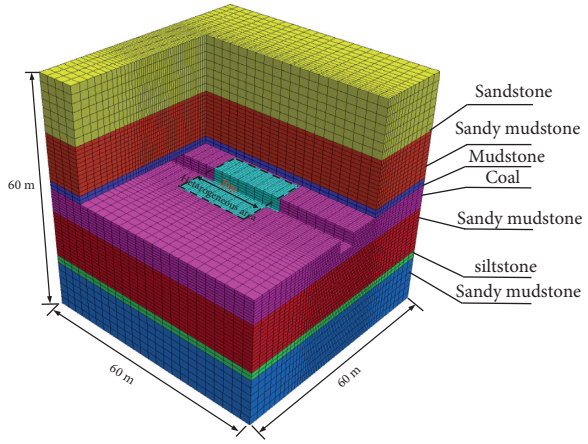


Figure 9: Heterogeneous model.

and analyzing the stability of roadways. The numerical model considering the heterogeneity of the rock mass provides calculation results closer to the field conditions, which verifies the correctness of the algorithm. This method can be used to study the stability and failure mechanism.

## 5. Effect of Rock Mass Heterogeneity on Underground Roadway Stability under Dynamic Loads

To study the stability of heterogeneous roadways under different dynamic loads, the roof deformation distribution, deformation magnitude, stress distribution, and surrounding rock plastic zone were monitored to show the effect of rock mass heterogeneity on the stability of the surrounding rock.

*5.1. Effect of Rock Mass Heterogeneity on Roof Deformation under Dynamic Loads.* Under dynamic loading conditions, spatial distribution of roof sag along roadway, in different $m$, is shown in Figure 16. Compared with the static loading conditions, the roof sag distribution shows variation under dynamic loads, and the deformation magnitude of the roof increases significantly. When $m = 1$, the maximum roof sag increases from 127.1 mm (PPV = 0.5 m/s) to 192.2 mm (PPV = 2.5 m/s). Average roof sag values for different dynamic loading conditions are shown in Table 5. According to Table 5 and Figure 16, the changes in $m$ directly influence the roof deformation magnitude and deformation distribution, and the influence changes with the increase in dynamic load strength. When PPV = 0.5 m/s, the maximum roof sag decreases with increasing $m$ from 127.1 to 48.6 mm; when PPV = 1.5 m/s, the maximum roof sag decreases from 156 to 56.2 mm; when PPV = 2.5 m/s, the maximum roof sag decreases from 192.2 to 78.9 mm. Under different dynamic loading conditions, the variation in the maximum roof sag caused by variations in heterogeneity is 78.5 mm, 99.8 mm, and 113.3 mm. These results show that the greater the dynamic load, the greater the impact of heterogeneity on the stability of surrounding rock.

To study the effect of the rock mass heterogeneity induced by heterogeneously distributed fractures on roof sags under different dynamic loads, values of roof deformation are captured from the model for different values of $m$. The deformation distribution pattern and the average roof sag under different dynamic loads are shown in Figure 17.

According to Figures 12 and 17(a), when PPV = 0.5 m/s, the deformation distribution pattern and the average roof sag are similar to those under static loads. With the increase in rock mass homogeneity, the difference in the average roof sag is 60.1 mm, and the difference is only 2.6 mm compared with the static loading conditions. As shown in Figure 17(a), the deformation distribution of the roof is mainly concentrated in the range of 30~59.9 mm, and the deformation of the entire roof is small. The effect of the dynamic loads (PPV = 0.5 m/s) on the roadway is lower when $m = 5$ and $m = 100$, and there is little change in the deformation distribution pattern.

As shown in Figure 17(b), when PPV = 1.5 m/s, the effect of dynamic loads on the deformation distribution pattern changes with increasing dynamic load strength. The effect of dynamic loads on roofs with different values of $m$ is obviously different. Compared with the deformation distribution pattern of the roof, when PPV = 0.5 m/s, the variation in the deformation distribution pattern becomes much larger when $m = 3$, and the proportion of the deformation distribution in the range of 30~59.9 mm increases by 50%.

As shown in Figure 17(c), when PPV = 2.5 m/s, the effect of dynamic loads on the deformation distribution pattern changes again. The deformation magnitude of the roof

Table 3: Rock mass properties.

| Lithology | $K$ (GPa) | $G$ (GPa) | $c$ (MPa) | $\Phi$ (°) | $c_r$ (MPa) | $\varepsilon_p$ (%) |
|---|---|---|---|---|---|---|
| Sandstone | 9.1 | 5.9 | 3.9 | 45 | 0.39 | 0.01 |
| Sandy mudstone | 5.2 | 3.1 | 3.2 | 40 | 0.32 | 0.01 |
| Mudstone | 2.4 | 1.1 | 2.1 | 35 | 0.21 | 0.01 |
| Coal | 1.3 | 0.6 | 1.4 | 31 | 0.14 | 0.01 |
| Sandy mudstone | 7.2 | 4.0 | 3.4 | 37 | 0.34 | 0.01 |
| Siltstone | 9.6 | 6.5 | 4.2 | 47 | 0.42 | 0.01 |

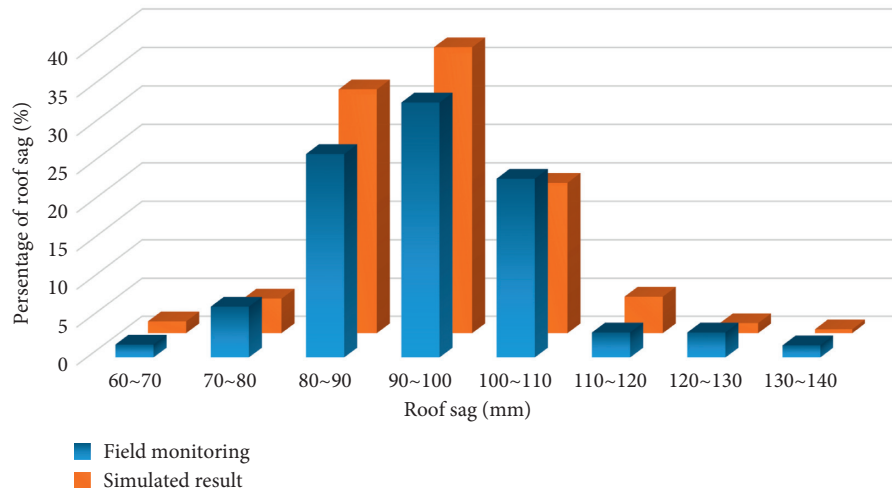


Figure 10: Statistics of roof sag values at different measuring points.

significantly increases with increasing dynamic load strength. The proportion of deformation distribution increases greatly in the range of 80~99.9 mm and 100~119.9 mm. With the increase in rock mass homogeneity, the variation difference of the average roof sag is 81.3 mm, and the difference is 21.2 mm compared with that at PPV = 0.5 m/s.

These results show that, under different dynamic loads the characteristics of the deformation distribution pattern are obviously different. When the dynamic load is low, the deformation distribution pattern is mainly determined by the degree of rock homogeneity, and the dynamic load has almost no effect on the deformation distribution pattern. The effect of dynamic loads on the deformation distribution pattern varies with increasing dynamic load strength. When the degree of rock mass heterogeneity is higher, the deformation distribution pattern is more easily affected by dynamic loads due to the relatively weak mechanical properties of the rock mass, and the deformation distribution will concentrate in the relatively large deformation range. Therefore, under a large dynamic loading condition, the deformation distribution pattern is determined by rock heterogeneity and dynamic load strength.

*5.2. Effect of Rock Mass Heterogeneity on Stress Distribution of Roof under Dynamic Loads.* Under dynamic loading conditions, the vertical stress distribution of the roof is shown in Figure 18. The relative size of the local stress reduction region in the roof is shown in Table 6. By comparing the relative size of the local stress reduction region under the same dynamic loading conditions, the area of the local stress reduction region of $t$ can be found. The roof decreases obviously with the increase of $m$, and the distribution of local stress will become uniform when $m = 100$.

When PPV = 0.5 m/s, the relative size of the stress reduction region decreases from 10.2% ($m = 1$) to 3.3% ($m = 5$), a decrease of 6.9%. When PPV = 1.5 m/s and PPV = 2.5 m/s, the relative size of the local stress reduction region caused by heterogeneous degree variation ($m = 1$ to $m = 5$) decreases by 11.1% and 22.5%, respectively. Note that when $m = 100$, with the increase in dynamic load strength, a stress reduction region appears along the central axis of the roof because the energy gathered in the roof is released after failure. Comparing with the vertical stress distribution of the roof under static loading conditions, it can be found that the effect of dynamic loads on the vertical stress distribution varies under different dynamic loads. According to the data analysis, the larger the dynamic load is, the more effect heterogeneity will have on roof stability.

*5.3. Effect of Rock Mass Heterogeneity on Plastic Zones under Dynamic Loads.* The plastic zone of the roadway at different positions under different dynamic loads is shown in Figure 19. By comparing Figures 15 and 19, the rock mass heterogeneity has a large effect on the plastic zone of the roadway under dynamic loads. The changes in $m$ directly influence the plastic zone extent at the roof and floor. To study the effect of the rock mass heterogeneity on the

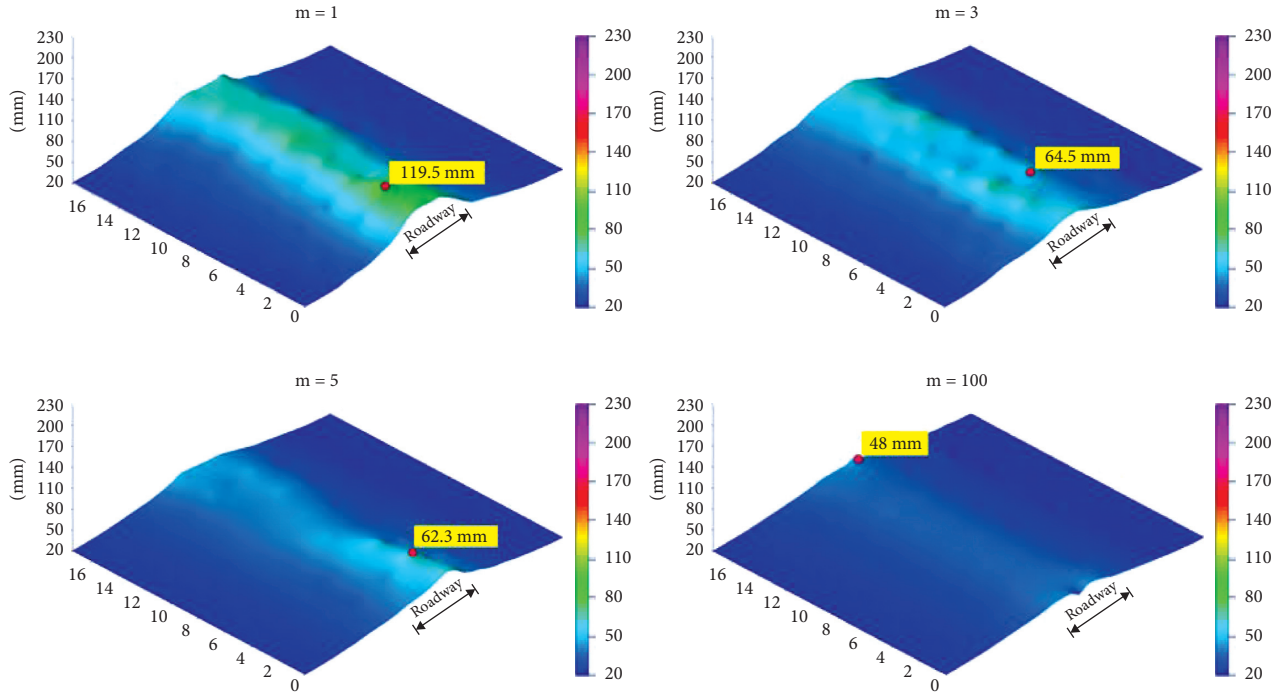


Figure 11: Roof sag distribution for different values of $m$ under static loads.

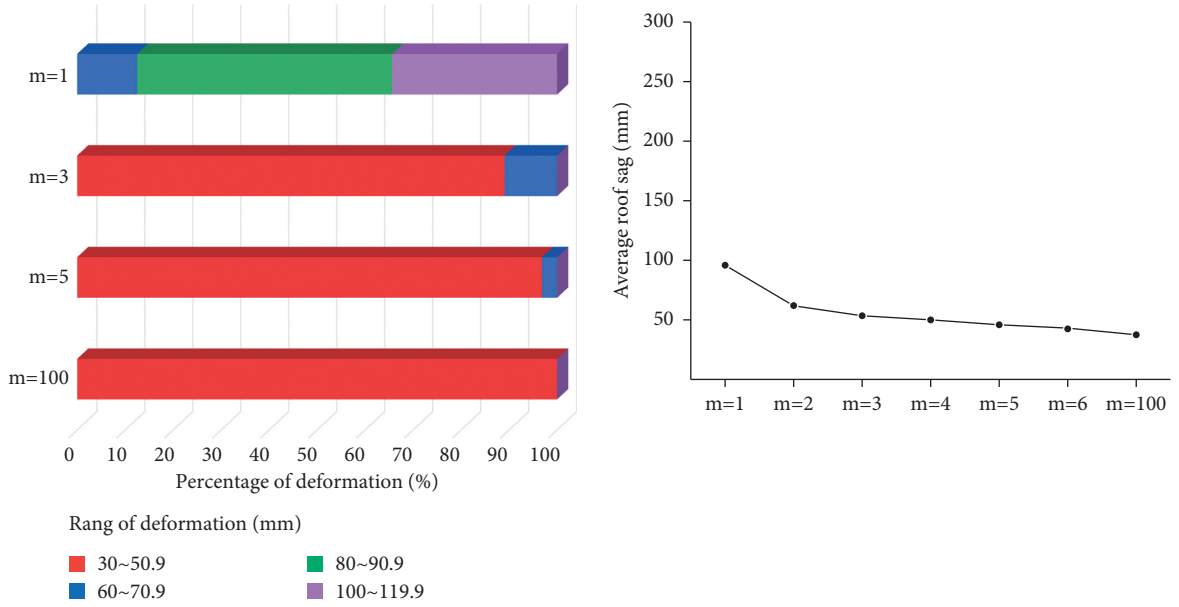


Figure 12: Roof deformation distribution pattern and the average roof sag for different values of $m$ under static loads.

roadway under different dynamic loads, the failure of the roadway at different positions under dynamic loads is analyzed. The plastic zone at 22 m is taken as an example for analysis. When PPV = 1.5 m/s, the plastic zone extent at the roof and the floor decreases from 5 m and 7.8 m to 4.0 m and 5.2 m, respectively, with an increase in $m$. When PPV = 2.5 m/s, the plastic zone extent at the floor decreases from 8.6 m to 6.9 m. These results show that the influence of rock mass heterogeneity on the plastic zone decreases with the increase of dynamic load strength.

Under different dynamic loading conditions, the number of failure elements in the plastic zone at 22 m of the roadway is shown in Table 7. As demonstrated with the data analyses and shown in Table 7, the number of failure elements in the plastic zone decreases with an increase in $m$. When PPV = 0 m/s, PPV = 1.5 m/s, and PPV = 2.5 m/s, the maximum variation differences in the amount of failure elements caused by variation in heterogeneity are 27, 76, and 81, respectively. The number of failure elements in the rock mass increases with increasing dynamic load strength.

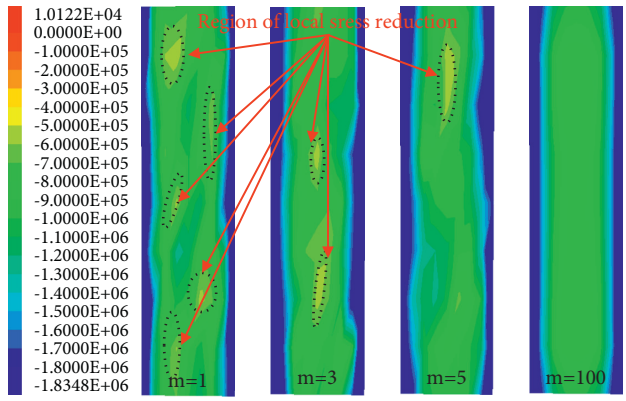


Figure 13: Roof vertical stress distribution under static loads.

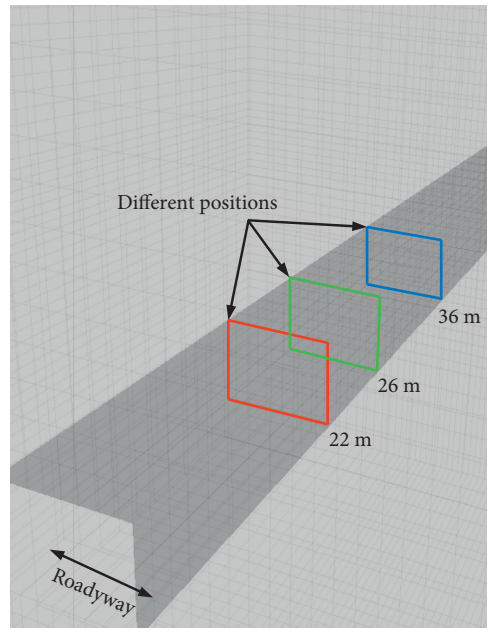


Figure 14: Monitoring sections at different positions of the roadway.

However, the effect of rock mass heterogeneity on the number of failure elements tends to weaken with increasing dynamic load strength.

According to the above analysis, the effect of rock mass heterogeneity on the stability of roadways significantly varies under dynamic loads. For deep roadways, under complicated conditions with high heterogeneity and frequent dynamic disturbance, it is necessary not only to analyze the effect of the heterogeneity of the rock mass on the stability of the roadway but also to study the effect of the dynamic loads on the stability of the heterogeneous roadway.

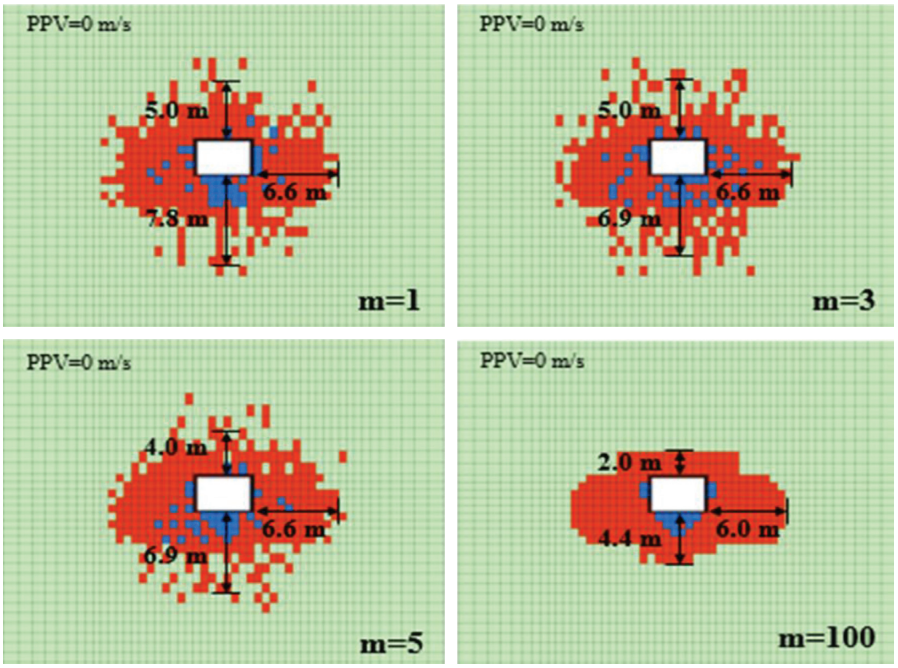


(a)

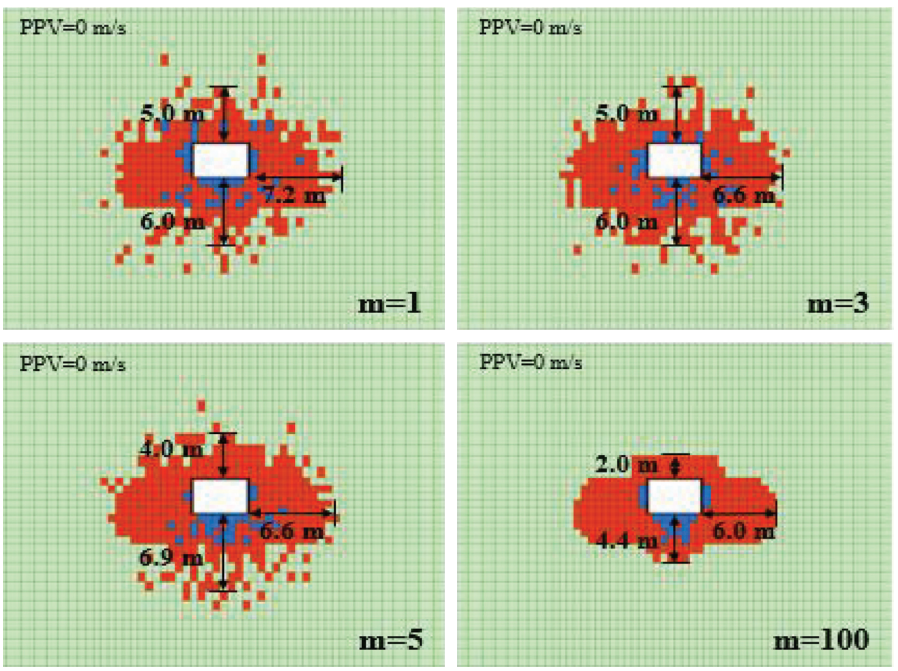


(b)

Figure 15: Continued.

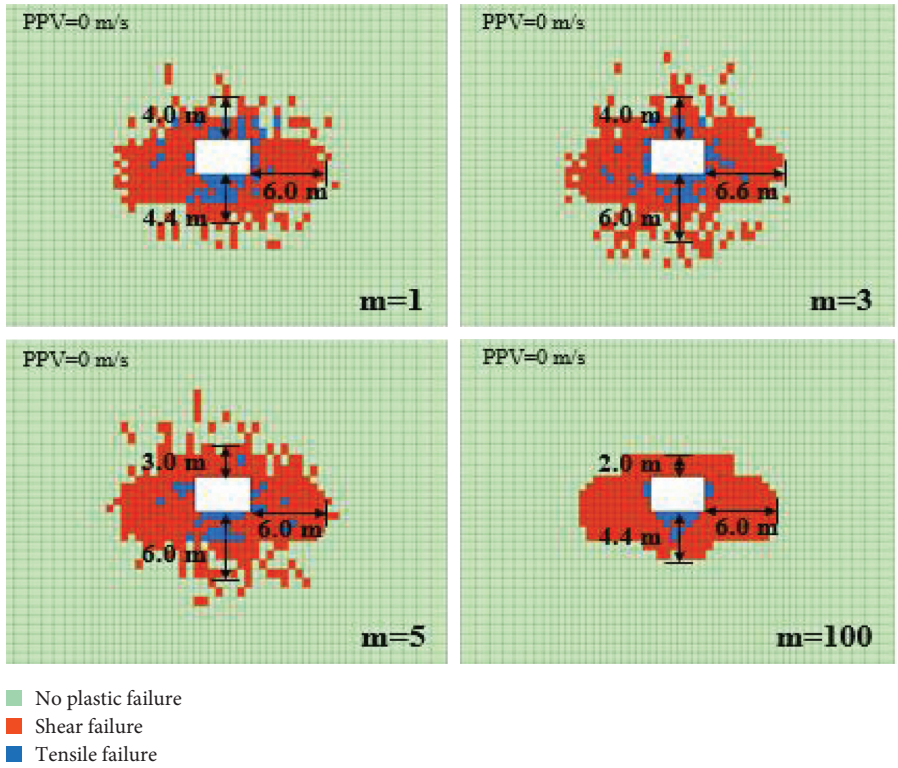


(c)

Figure 15: Plastic zones under static loads at different positions of the roadway: (a) 22 m, (b) 26 m, and (c) 36 m.

Table 4: The number of failure elements at different positions for different values of $m$.

| $m$ | Positions (m) | Number of failure elements |
|---|---|---|
| 1 | 22 | 329 |
| | 26 | 526 |
| | 36 | 303 |
| | 22 | 320 |
| 5 | 26 | 324 |
| | 36 | 328 |
| | 22 | 249 |
| 100 | 26 | 238 |
| | 36 | 250 |

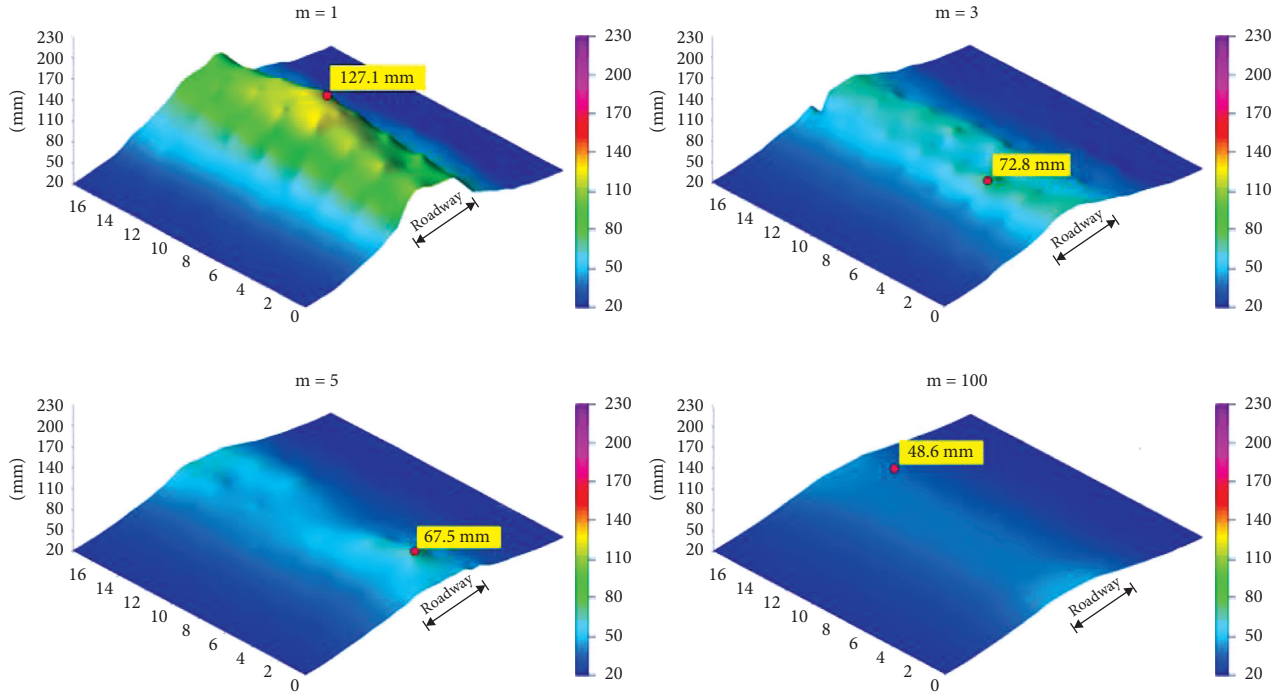


(a)

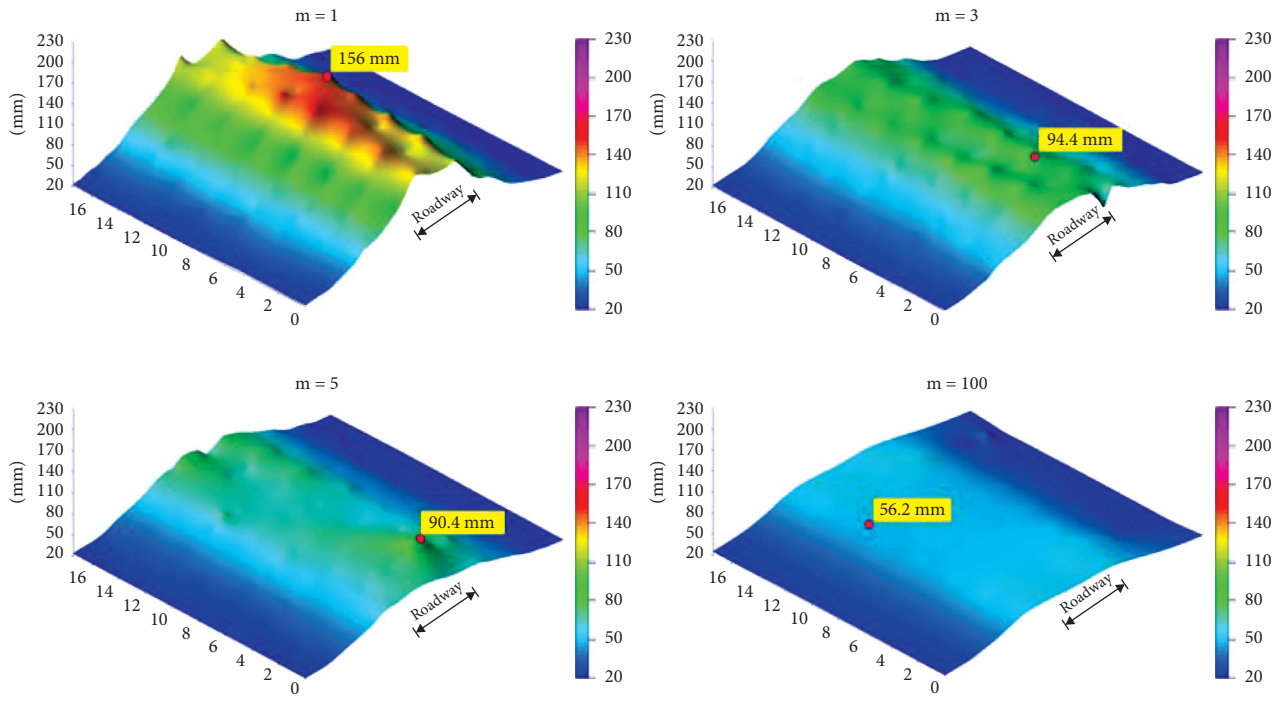


(b)

Figure 16: Continued.

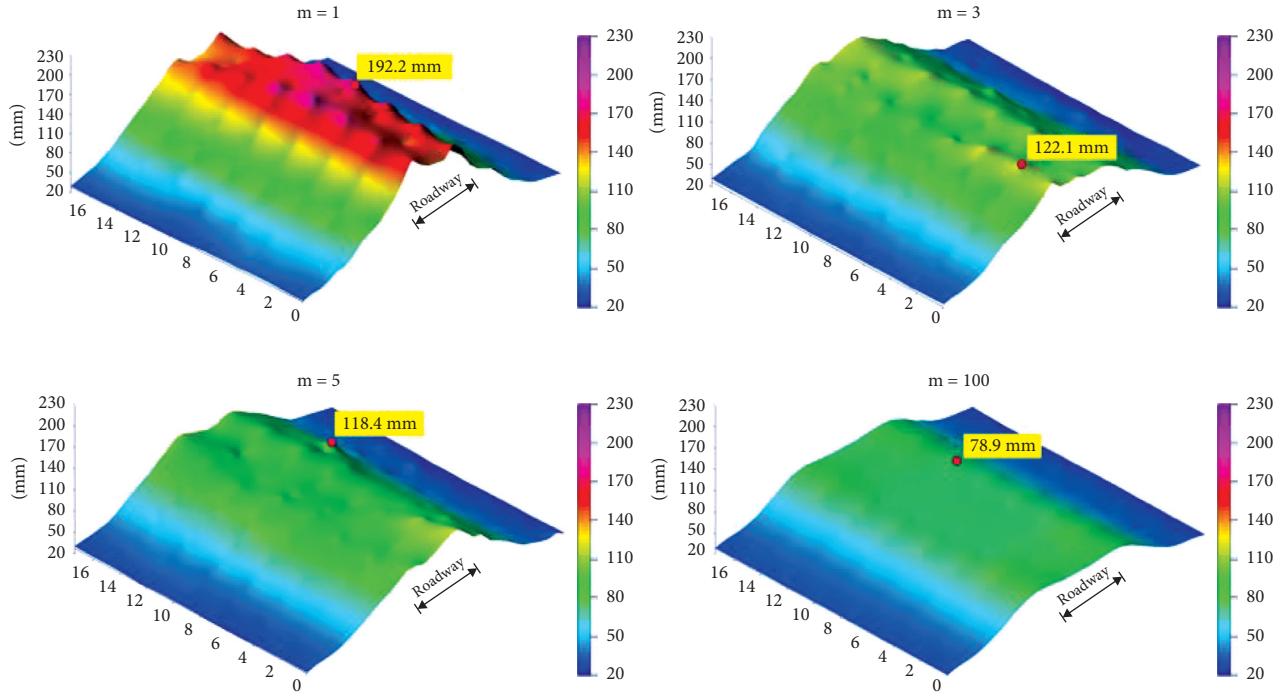


(c)

Figure 16: Roof sag distribution for different values of $m$ under dynamic loads: (a) PPV = 0.5 m/s, (b) PPV = 1.5 m/s, and (c) PPV = 2.5 m/s.

Table 5: The average roof sag under the different dynamic loads.

| PPV (m/s) | The average roof sag (mm) $m$ | | | |
|---|---|---|---|---|
| | 1 | 3 | 5 | 100 |
| 0 | 95.1 | 53.0 | 46.2 | 37.6 |
| 0.5 | 102.5 | 59.4 | 51.8 | 42.4 |
| 1.5 | 129.3 | 79.8 | 69.8 | 54.1 |
| 2.5 | 158.2 | 107.2 | 94.7 | 76.9 |

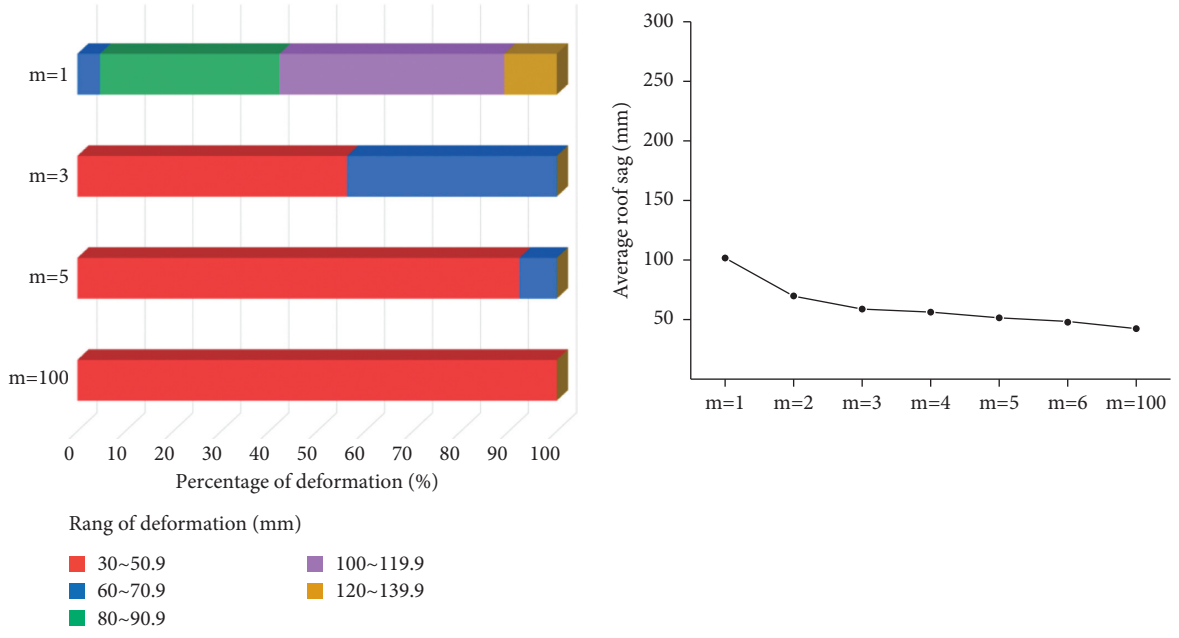


(a)

Figure 17: Continued.

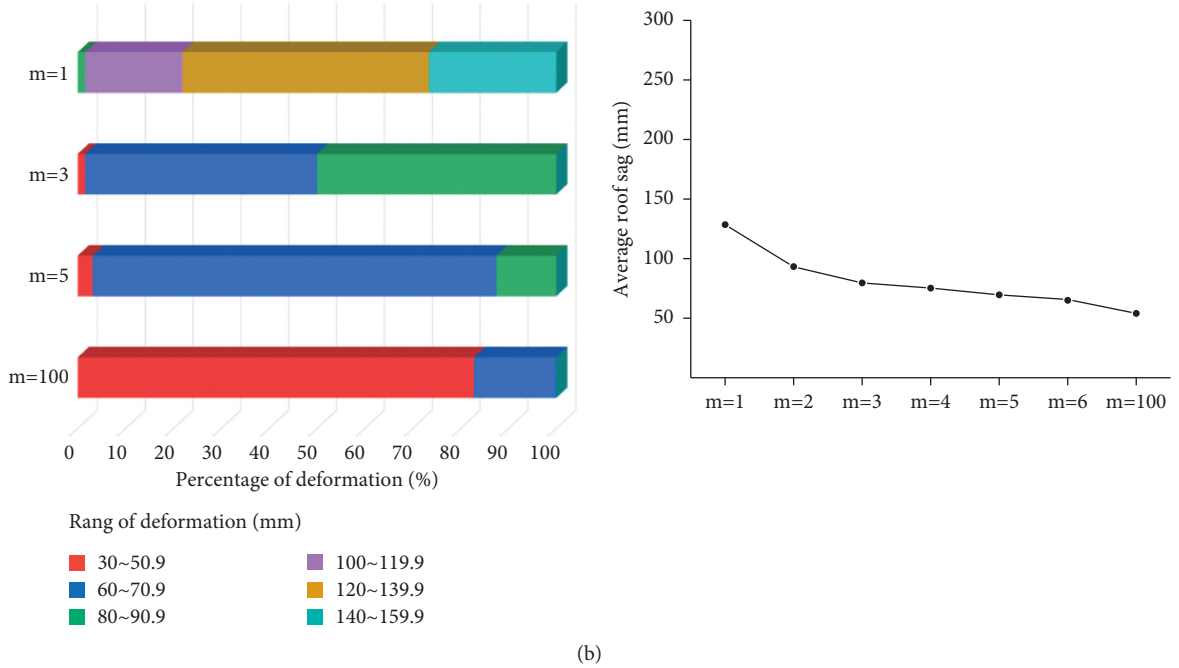


(b)

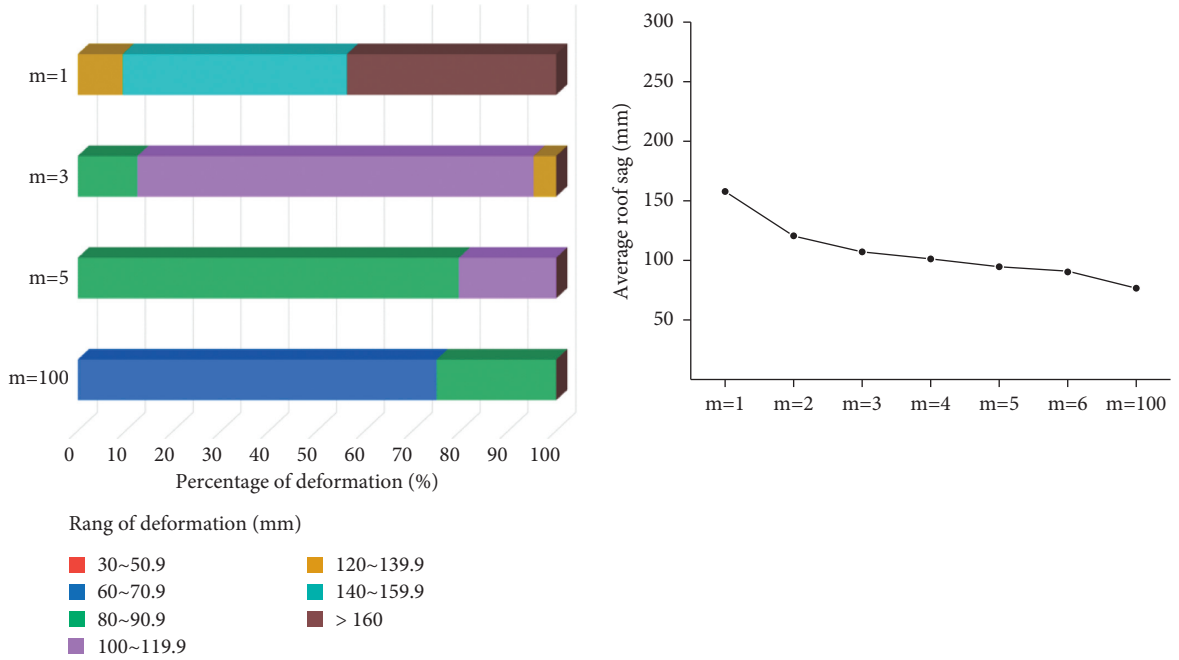


(c)

FIGURE 17: Roof deformation distribution pattern and the average roof sag with respect to $m$ under different dynamic loads: (a) PPV = 0.5 m/s, (b) PPV = 1.5 m/s, and (c) PPV = 2.5 m/s.

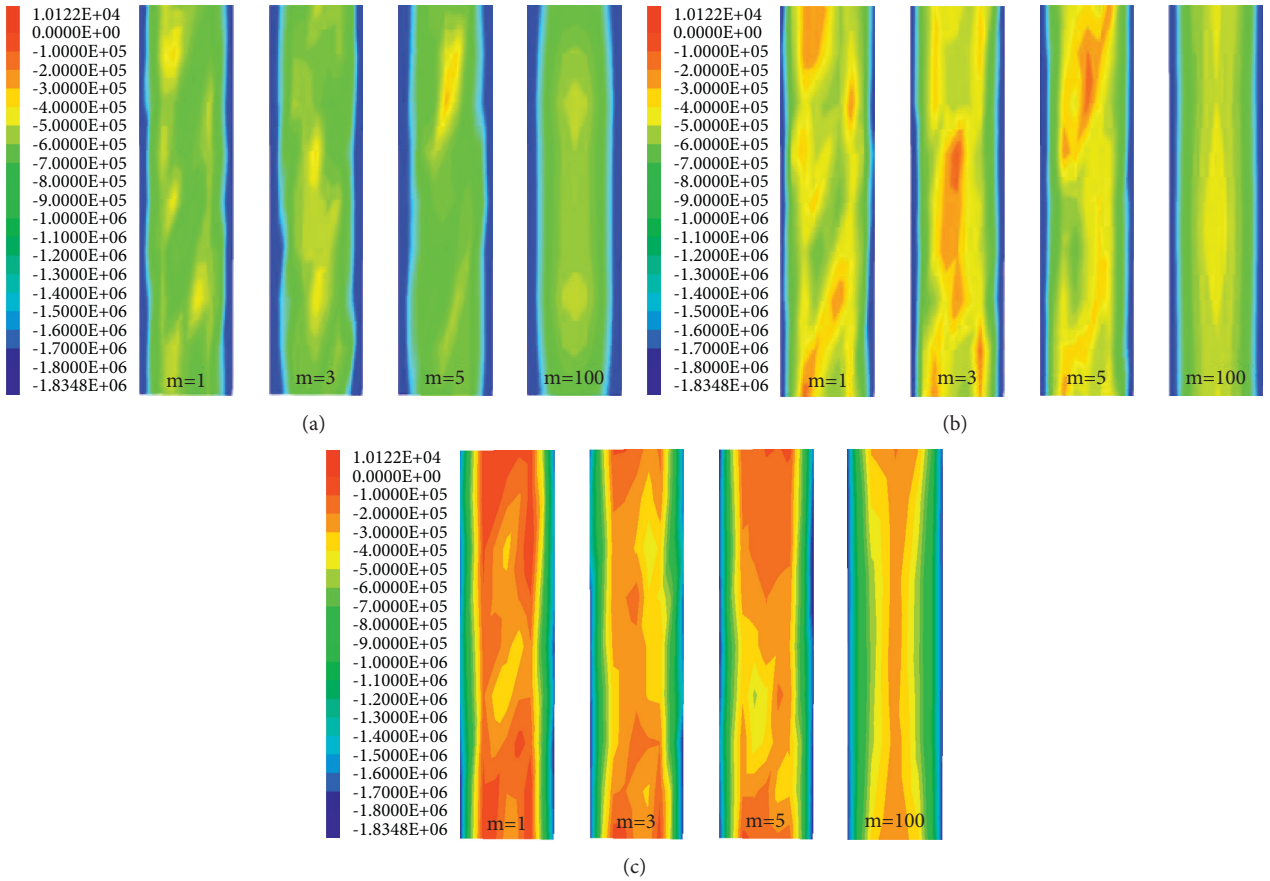


Figure 18: Roof vertical stress distribution under different dynamic loads: (a) PPV = 0.5 m/s, (b) PPV = 1.5 m/s, and (c) PPV = 2.5 m/s.

Table 6: The relative size (percentage of total area) of the local stress reduction region under different dynamic loads.

| PPV (m/s) | The relative size of local stress reduction region (%) | | | |
|---|---|---|---|---|
| | $m$ | | | |
| | 1 | 3 | 5 | 100 |
| 0.5 | 10.2 | 11.0 | 3.8 | 0 |
| 1.5 | 16.5 | 10.8 | 5.3 | 0 |
| 2.5 | 38.6 | 10.8 | 16 | 0 |

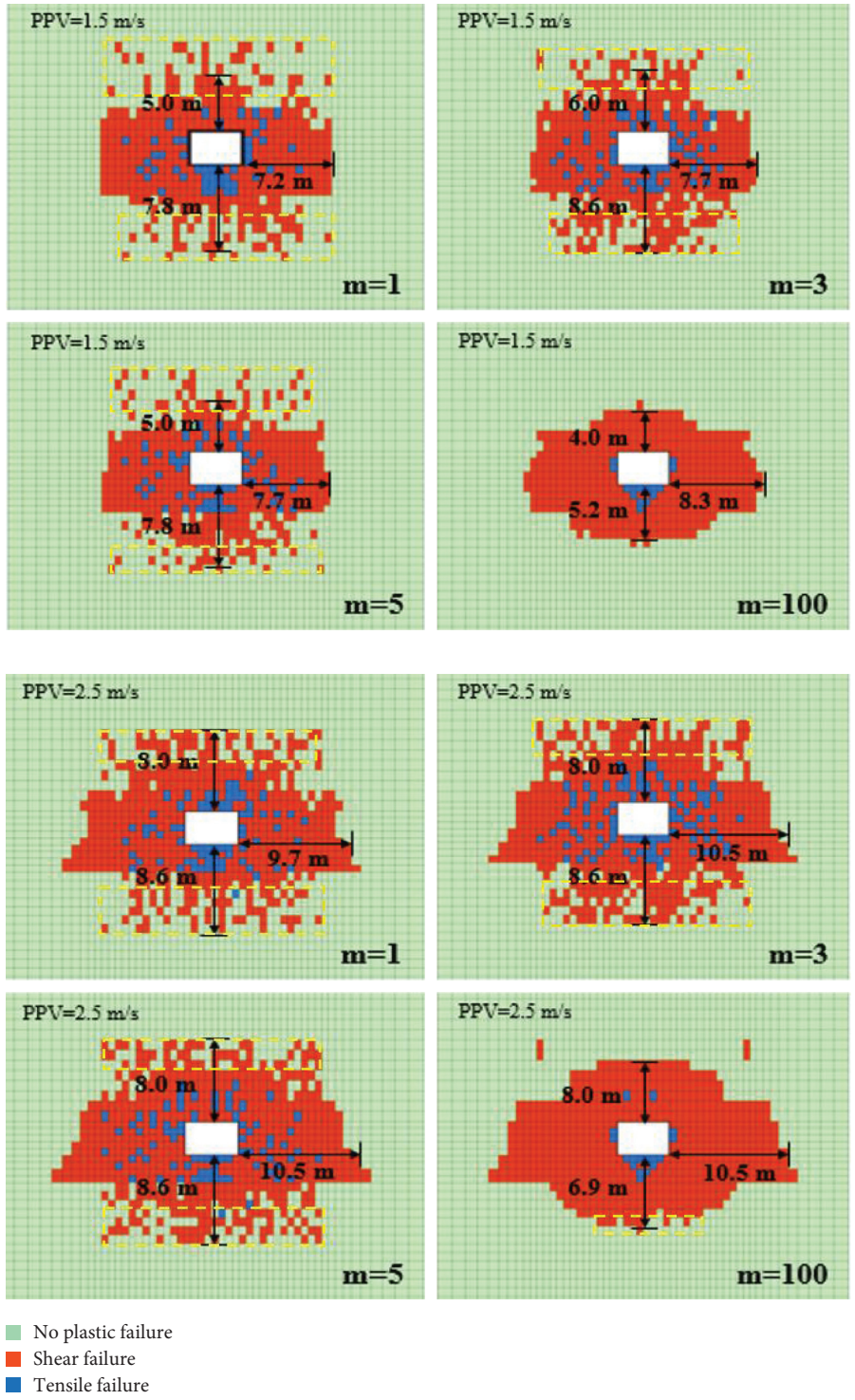


(a)

Figure 19: Continued.

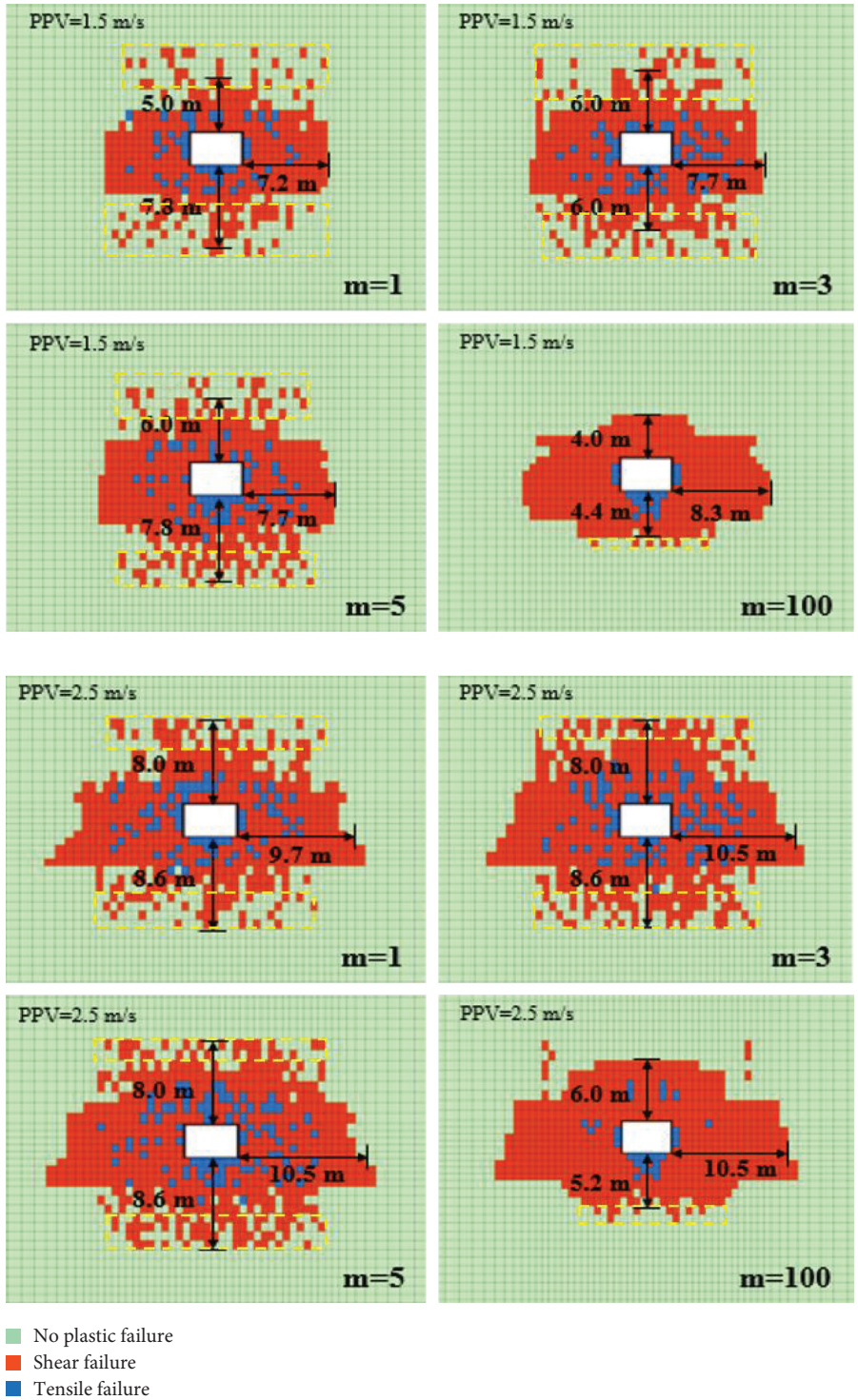


(b)

Figure 19: Continued.

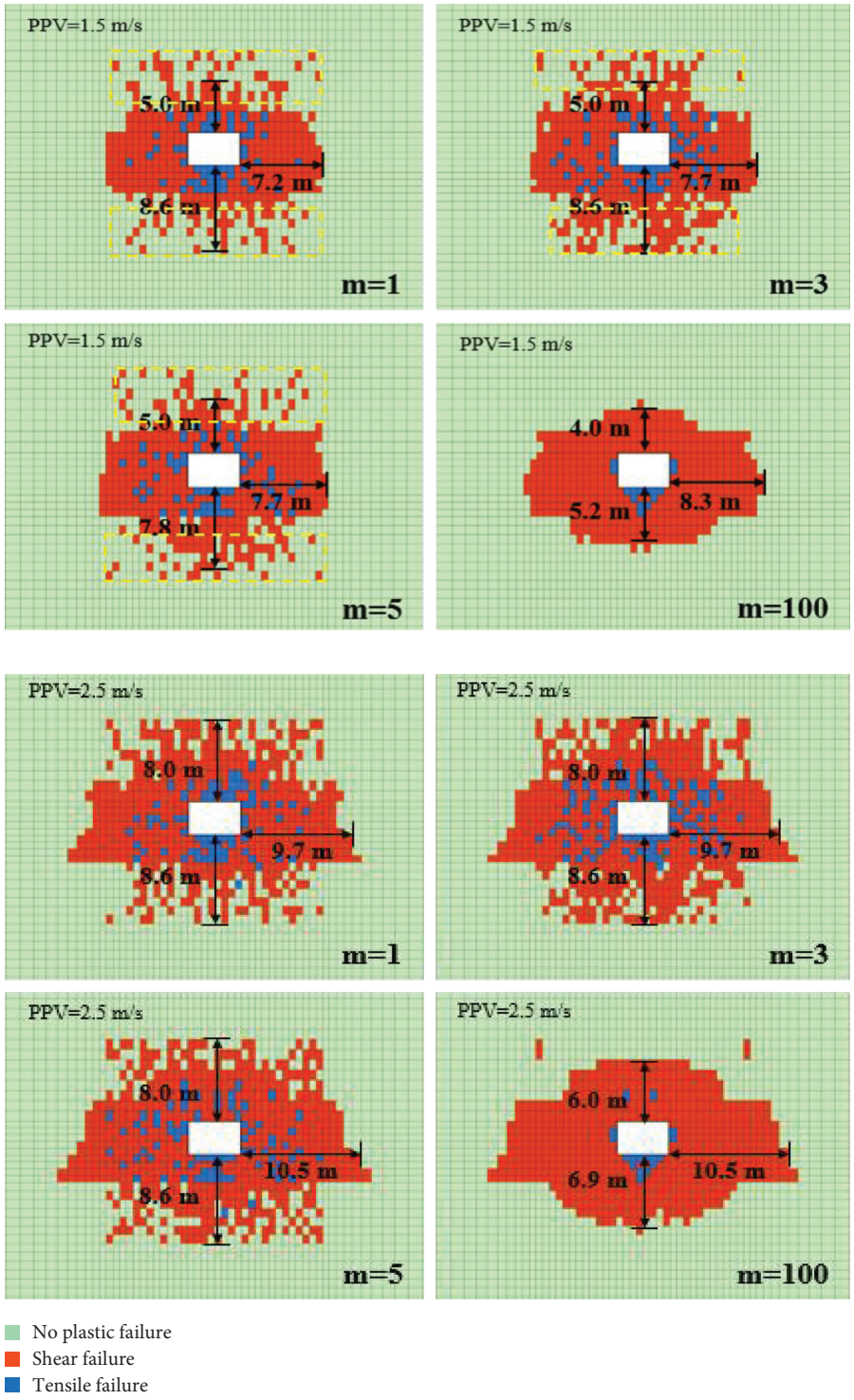


(c)

Figure 19: Plastic zone of the roadway at different positions under different dynamic loads: (a) 22 m, (b) 26 m, and (c) 36 m.

Table 7: The number of failure elements at the 22 m position of the roadway with respect to $m$.

| PPV (m/s) | $m$ | Number of failure elements |
|---|---|---|
| 0 | 1 | 329 |
| | 3 | 347 |
| | 5 | 320 |
| | 100 | 249 |
| 1.5 | 1 | 452 |
| | 3 | 509 |
| | 5 | 499 |
| | 100 | 433 |
| 2.5 | 1 | 636 |
| | 3 | 707 |
| | 5 | 717 |
| | 100 | 650 |

## 6. Conclusions

Based on the engineering background of Zhaogu No. 2 Mine, this paper uses a Weibull distribution model to describe the heterogeneous rock mass, studying the effect of heterogeneity on the rock mass by FLAC3D numerical simulation software. The effects of rock mass heterogeneity on the deformation, stress distribution, and plastic zones of the roadway effect are analyzed. The results show that, under static loads, the positions of the maximum sag have significant randomness, and the average roof sag gradually decreases with an increase in $m$. As $m$ increases, the maximum roof sag decreases from 119.5 mm ($m = 1$) to 48 mm ($m = 100$). Under dynamic loads, the effect of variations in heterogeneity is found to change. With the increase in dynamic load strength, the change in variation difference of the sag value caused by variations in heterogeneity will increase.

After roadway excavation, the roof is affected by the heterogeneity of the rock mass, forming a region where the stress decreases locally. Under static loads, as the rock mass becomes more homogeneous, the vertical stress distribution tends to be uniformly distributed. The percentage of stress reduction region in roof decreases from 9.4% ($m = 1$) to 2.8% ($m = 5$). Under dynamic loads, this effect caused by variation in heterogeneity becomes much larger. When PPV = 0.5 m/s, the relative size of the stress reduction region decreases from 10.2% ($m = 1$) to 3.3% ($m = 5$), a decrease of 6.9%. When PPV = 1.5 m/s and PPV = 2.5 m/s, the relative size of the local stress reduction region caused by heterogeneous degree variation ($m = 1$ to $m = 5$) decreases by 11.1% and 22.5%, respectively.

Rock mass heterogeneity in the plastic zones of roadways at different positions is investigated. Under static loads, the plastic zones at different positions of the roadway are significantly different when the heterogeneity of the rock mass is considered. Under dynamic loads, this effect of variations in heterogeneity is found to change. The number of failure elements in the rock mass increases with increasing dynamic load strength, but the rate of increase tends to decrease with increasing dynamic load strength.

## Data Availability

The data used to support the findings of this study are available from the corresponding author upon request.

## Conflicts of Interest

The authors declare that they have no conflicts of interest.

## Acknowledgments

This study was financially supported by the National Natural Science Foundation of China (52074166 and 51774195) and the China Postdoctoral Science Foundation (2019M652436).

## References

[1] M. He, X. Lu, and H. Jing, "Characters of surrounding rock mass in deep engineering and its non-linear dynamic-mechanical design concept," *Chinese Journal of Rock Mechanics and Engineering*, vol. 21, no. 8, pp. 1215–1224, 2002.

[2] Q. Qi, Y. Pan, and L. I. Hai-tao, "Theoretical basis and key technology of prevention and control of coal-rock dynamic disasters in deep coal mining," *Journal of China Coal Society*, vol. 45, no. 5, pp. 1567–1584, 2020.

[3] W. C. Zhu, Z. H. Li, L. Zhu, and C. A. Tang, "Numerical simulation on rockburst of underground opening triggered by dynamic disturbance," *Tunnelling and Underground Space Technology*, vol. 25, no. 5, pp. 587–599, 2010.

[4] P. Kong, L. Jiang, J. Shu, and L. Wang, "Mining stress distribution and fault-slip behavior: a case study of fault-influenced longwall coal mining," *Energies*, vol. 12, no. 13, p. 2494, 2019.

[5] G. Wang, S. Gong, L. Dou, W. Cai, X. Yuan, and C. Fan, "Rockburst mechanism and control in coal seam with both syncline and hard strata," *Safety Science*, vol. 115, pp. 320–328, 2019.

[6] L. Wang, A. Cao, L. Dou et al., "Numerical simulation on failure effect of mining-induced dynamic loading and its influential factors," *Safety Science*, vol. 113, pp. 372–381, 2019.

[7] X. Liu, D. Fan, Y. Tan et al., "Failure evolution and instability mechanism of surrounding rock for close-distance parallel chambers with super-large section in deep coal mines," *International Journal of Geomechanics*, vol. 21, no. 5, Article ID 04021049, 2021.

[8] X. Liu, S. Song, Y. Tan et al., "Similar simulation study on the deformation and failure of surrounding rock of a large section chamber group under dynamic loading," *International Journal of Mining Science and Technology*, vol. 31, no. 3, pp. 495–505, 2021.

[9] X. Liu, D. Fan, Y. Tan, and J Ning, "New detecting method on the connecting fractured zone above the coal face and a case study," *Rock Mechanics and Rock Engineering*, vol. 202113 pages, 2021.

[10] J. He, L. Dou, Z. Li, and Y. Ding, "Mechanism of dynamic and static combined load inducing rock burst in thin coal seam," *Journal of China Coal Society*, vol. 39, no. 11, pp. 2177–2182, 2014.

[11] P. Kong, M. Jiang, and W. Chen, "Numerical analysis of roadway rock-burst hazard under superposed dynamic and static loads," *Energies*, vol. 12, no. 19, p. 3761, 2019.

[12] S. Liu, "Nonlinear catastrophy model and chaotic dynamic mechanism of compound coal-rock unstable failure under

coupled static-dynamic loading," *Journal of China Coal Society*, vol. 39, no. 2, pp. 292–300, 2014.

[13] H. Lan, C. D. Martin, and H. Bo, "Effect of heterogeneity of brittle rock on micromechanical extensile behavior during compression loading," *Journal of Geophysical Research Solid Earth*, vol. 115, Article ID B006496, 14 pages, 2010.

[14] T.-M. He, Q. Zhao, J. Ha, K. Xia, and G. Grasselli, "Understanding progressive rock failure and associated seismicity using ultrasonic tomography and numerical simulation," *Tunnelling and Underground Space Technology*, vol. 81, pp. 26–34, 2018.

[15] M. C. Villeneuve, M. S. Diederichs, and P. K. Kaiser, "Effects of grain scale heterogeneity on rock strength and the chipping process," *International Journal of Geomechanics*, vol. 12, no. 6, pp. 632–647, 2012.

[16] B. Han, G. Zhang, H. Lan, and C Yan, "Geometrical heterogeneity of the joint roughness coefficient revealed by 3D laser scanning," *Engineering Geology*, vol. 265, Article ID 105415, 2019.

[17] A. Manouchehrian and M. Cai, "Influence of material heterogeneity on failure intensity in unstable rock failure," *Computers and Geotechnics*, vol. 71, pp. 237–246, 2016.

[18] H. Yoshida, D. Takamori, and M. Wada, "Study on effect of material heterogeneity on behaviors of rock structure and its design," *Journal of Applied Mechanics*, vol. 2010, no. 387, Article ID 6387, 2010.

[19] L. F. Fan, F. Ren, and G. W. Ma, "Experimental study on viscoelastic behavior of sedimentary rock under dynamic loading," *Rock Mechanics and Rock Engineering*, vol. 45, no. 3, pp. 433–438, 2012.

[20] G. Pappalardo, R. Punturo, S. Mineo, and L. Contrafatto, "The role of porosity on the engineering geological properties of 1669 lavas from Mount Etna," *Engineering Geology*, vol. 221, pp. 16–28, 2017.

[21] L. Peng, J. Yang, P. G. Ranjith, Z. Zheng, and J. Chen, "Experimental investigation of the effects of heterogeneity and geostress difference on the 3D growth and distribution of hydrofracturing cracks in unconventional reservoir rocks," *Journal of Natural Gas Science and Engineering*, vol. 35, pp. 541–554, 2016.

[22] H. F. Schweiger, R. Thurner, and R. Pöttler, "Reliability analysis in geotechnics with deterministic finite elements - theoretical concepts and practical application," *International Journal of Geomechanics*, vol. 1, no. 4, pp. 389–413, 2001.

[23] K.-I. Song, G.-C. Cho, and S.-W. Lee, "Effects of spatially variable weathered rock properties on tunnel behavior," *Probabilistic Engineering Mechanics*, vol. 26, no. 3, pp. 413–426, 2011.

[24] P. Kong, L. Jiang, J. Shu, A. Sainoki, and Q. Wang, "Effect of fracture heterogeneity on rock mass stability in a highly heterogeneous underground roadway," *Rock Mechanics and Rock Engineering*, vol. 52, no. 11, pp. 4547–4564, 2019.

[25] L. Jiang, A. Sainoki, H. S. Mitri, N. Ma, H. Liu, and Z. Hao, "Influence of fracture-induced weakening on coal mine gateroad stability," *International Journal of Rock Mechanics and Mining Sciences*, vol. 88, pp. 307–317, 2016.

[26] W. Weibull, "A statistical distribution function of wide applicability," *Journal of Applied Mechanics*, vol. 18, no. 3, pp. 293–297, 1951.

[27] A. Paluszny, X. Tang, M. Nejati, and R. W. Zimmerman, "A direct fragmentation method with Weibull function distribution of sizes based on finite- and discrete element simulations," *International Journal of Solids and Structures*, vol. 80, pp. 38–51, 2016.

[28] C. A. Tang, H. Liu, P. K. K. Lee, Y. Tsui, and L. G. Tham, "Numerical studies of the influence of microstructure on rock failure in uniaxial compression - part I: effect of heterogeneity," *International Journal of Rock Mechanics and Mining Sciences*, vol. 37, no. 4, pp. 555–569, 2000.

[29] J. A. Hudson and C. Fairhurst, "Tensile strength, weibull's theory and a general statistical approach to rock failure," in *Proceedings of the Civil Engineering Materials Conference*, London, UK, USA, 1969.

[30] L. Jiang, P. Zhang, L. Chen et al., "Numerical approach for goaf-side entry layout and yield pillar design in fractured ground conditions," *Rock Mechanics and Rock Engineering*, vol. 50, no. 11, pp. 3049–3071, 2017.

[31] E. Hoek, "Hoek-Brown failure criterion-2002 edition," *Proceedings of NARMS-Tac*, vol. 1, pp. 18–22, 2002.

[32] Z. Yuan, Z. Cao, Y. Cai, X. Geng, and X. Wang, "An analytical solution to investigate the dynamic impact of a moving surface load on a shallowly-buried tunnel," *Soil Dynamics and Earthquake Engineering*, vol. 126, Article ID 105816, 2019.

[33] J. Xu, R. Zhou, D. Song, N. Li, K. Zhang, and D. Xi, "Deformation and damage dynamic characteristics of coal-rock materials in deep coal mines," *International Journal of Damage Mechanics*, vol. 28, no. 1, pp. 58–78, 2017.

[34] J. He, L.-M. Dou, W. Cai, Z.-L. Li, and Y.-L. Ding, "In situ test study of characteristics of coal mining dynamic load," *Shock and Vibration*, vol. 2015, Article ID 121053, 8 pages, 2015.